CRYSTAL Research & Technology

Cryst. Res. Technol. 51, No. 8, 466–474 (2016) / DOI 10.1002/crat.201600068

Original Paper

Growth of carbon nanotubes from waste blast furnace gases at atmospheric pressure

Jagdeep S. Sagu[1], K.G. Upul Wijayantha[1,], Paul Holland[2], Mallika Bohm[3], Siva Bohm[3], Tapan Kumar Rout[4], and Hemaka Bandulasena[5]*

Received 29 February 2016, accepted 20 June 2016
Published online 14 July 2016

Carbon emissions from industrial sources are of major global concern, especially contributions from the steel manufacturing process which accounts for the majority of emissions. Typical blast furnace gases consist of CO_2 (20-25%), CO (20-25%), H_2 (3-5%) and N_2 (40-50%) and trace amounts of other gases. It is demonstrated that gas mixtures with these compositions can be used at atmospheric pressure to grow carbon nanotubes (CNTs) by chemical vapor deposition (CVD) on to steel substrates, which act as catalysts for CNT growth. Computational modelling was used to investigate the CNT growth conditions inside the CVD chamber. The results show that industrial waste pollutant gases can be used to manufacture materials with significant commercial value, in this case CNTs.

1 Introduction

Greenhouse gas emissions are having a noticeable effect on the global climate, and if the current trend continues, there could be significant economic, environmental and social implications in the future. Of the six greenhouse gases (H_2O, CO_2, CH_4, N_2O, O_3 and CFCs) covered in the Kyoto protocol, CO_2 is the key contributor posing a significant threat. [1] It is widely known that the majority of the CO_2 emissions originate from the iron and steel industry, where iron oxides are converted to molten iron in a blast furnace, emitting vast quantities of CO_2 and carbon monoxide (CO), which are known as blast furnace gases. The total world steel production is in excess of 10,000 billion tons. On average, the steel industry produces around 1.9 tons of CO_2 per ton of steel produced. [2] Whilst there are many studies on the capture and storage of CO_2, [3] it is more desirable to convert CO_2 into a value added commodity or chemical feed-stock.

Carbon nanotubes (CNTs) have recently been used in many diverse applications such as sensors, [4] ceramics, [5] filters and membranes, [6] catalysis [7] and energy storage devices, [8–10]. If the CO_2 and CO from the waste blast furnace gases could be utilized as the carbon source for CNT growth, it will be an economically viable process and a sustainable technology. The fact that billions of tons of blast furnace gases (which have 'no value' or 'negative value') are produced every year makes its conversion to CNTs highly appealing, considering that the current global CNT market is worth over 5 billion USD with an expected annual increase of 12% over the next few years. [11, 12]

There are very few reports on the use of CO as the main carbon source for synthesis of carbon nanotubes. [13–16] Whilst CO is usually present in many CVD gas mixtures for synthesis of CNTs, its role is that of a reducing agent rather than the main source of carbon. However, reduction of CO_2 to carbon is more difficult and challenging because it is a kinetically and thermodynamically stable molecule, [17] nevertheless, it has been used to grow CNTs by other methods. [18–21]. To the best of

* Corresponding author: E-mail: U.Wijayantha@lboro.ac.uk
Tel: +44 (0) 1509 222574, Fax: +44 1509 223925

[1] Energy Research Laboratory, Department of Chemistry, Loughborough University, Loughborough LE11 3TU, United Kingdom
[2] EffecTech Ltd, Dove House, Dove Fields, Uttoxeter, Staffordshire ST14 8HU, United Kingdom
[3] TATA Steel R&D, Swinden Technology Centre, Moorgate, Rotherham S60 3AR, United Kingdom
[4] New Technology Developments & Strategy Planning Research & Development Division, TATA Steel Ltd. Jamshedpur 831007, India
[5] Department of Chemical Engineering, Loughborough University, Loughborough LE11 3TU, United Kingdom

CRYSTAL Research & Technology

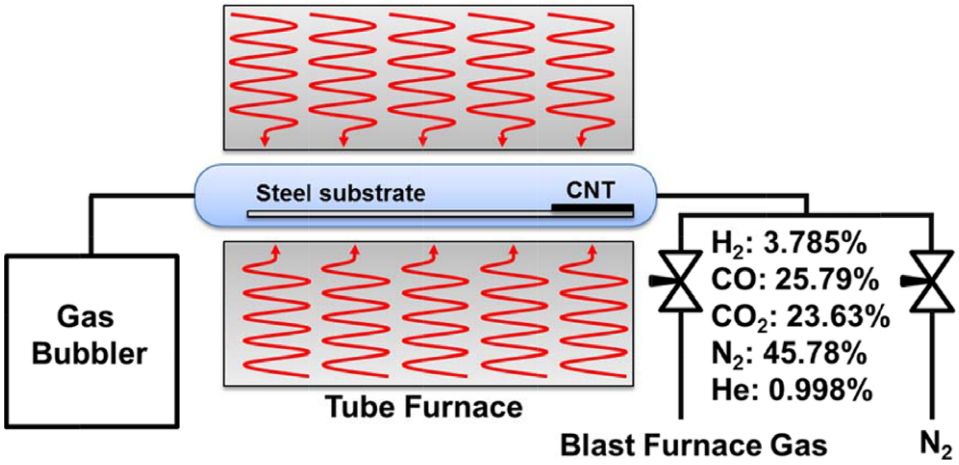

Fig. 1 Experimental setup for CVD of blast furnace gas to produce CNTs.

our knowledge, there are no reports on the growth of carbon nanotubes from waste blast furnace gases.

In this study, we report the growth of CNTs on steel substrates at atmospheric pressure using gas mixtures that closely resemble that of the waste blast furnace gases. We believe that in our process, the steel substrate acts as the catalyst for the growth of CNTs as reported by Gaikwad *et al.* recently. [22] From the end user view point, growth of CNTs directly on to steel substrates is very attractive as they have direct applications as electrodes in Li-ion batteries, supercapacitors and bipolar plates in fuel cells, [8–10, 23]. It was found that the CNTs have only grown at the front end of the steel substrate where the density is just high enough to provide a sufficient collision frequency of the carbon source molecules with the steel substrate. To validate this hypothesis, CFD simulations were conducted in order to determine the flow and temperature profiles within the tube furnace. The simulations have indicated that at the front end of the tube where the CNT growth has taken place, the temperature and hence the density of the gas varies significantly, suggesting that it could be the main reason for the CNT coating to occur.

2 Experimental

2.1 Sample preparation by CVD of blast furnace gas over a steel substrate

The cold rolled steel substrates (Q-panel) were cut in to 100×15 mm sized strips and were ultrasonically cleaned in isopropanol and acetone for 15 mins prior to the growth to remove any grease from the surface. The strip was then placed in a quartz tube inside a tube furnace. One end of the quartz tube was connected to a gas bubbler filled with water; the other end was connected to a three-way switch valve which linked a nitrogen cylinder and a cylinder containing a gas mixture which mimics the blast furnace gas (composition: H_2: 3.785%, CO: 25.79%, CO_2: 23.65%, N_2: 45.78% and He: 0.998%). The composition of the gases was confirmed by gas chromatography. The CNT growth setup is shown in figure 1. First, the quartz tube was purged with N_2 at a flow rate of 800 ml/min for 15 mins, and then the furnace was heated whilst maintaining the N_2 purging. When the desired furnace set temperature (825 °C) was reached, the gas flow was switched to the blast furnace gas mixture at a flow rate of 250 ml/min and was maintained for 30 mins. Once the deposition was completed, the gas flow was switched back to the nitrogen flow and the furnace was allowed to cool down to room temperature.

2.2 Instrumentation

Carbon coated steel samples were characterised by Raman spectroscopy, FEGSEM and TEM. Raman spectroscopy was carried out using a HORIBA Jobin Yvon LabRAM HR (with 632.8 nm He-Ne laser) Raman spectrophotometer. The spectrum was recorded in the range of 100–3100 cm^{-1}. The surface morphology of the steel samples was studied using a Leo 1530 VP field emission gun scanning electron microscope (FEGSEM) at an accelerating voltage of 5 kV and a working distance of 5 mm. TEM images were taken using a JEOL JEM – 2000FX TEM. For TEM, the sample was prepared by scraping the carbon nanotubes from the steel substrate, and then suspending in ethanol. The suspension was sonicated for 30 mins and then the Cu TEM grid was

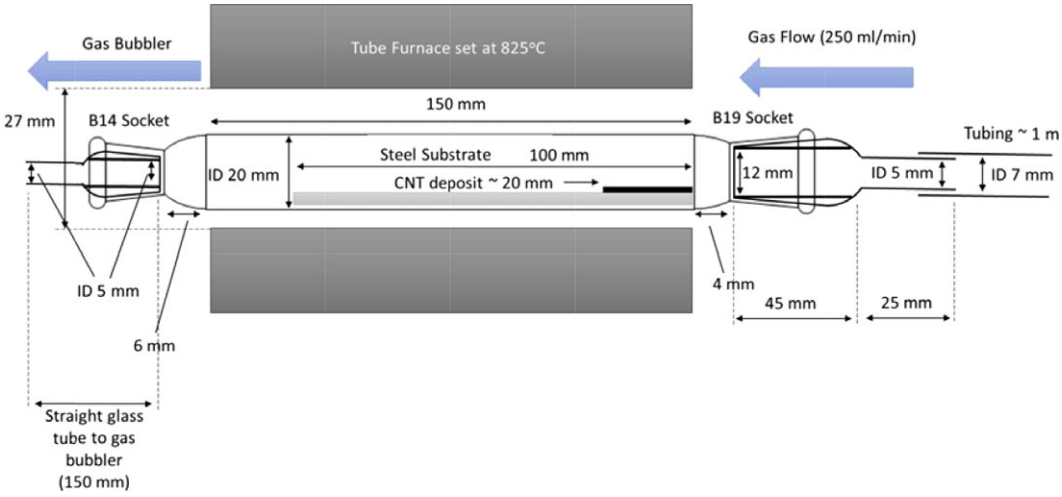

Fig. 2 Detailed schematic diagram showing the measurements of the CVD setup.

dipped in to the suspension in order to facilitate the adherence of carbon nanotubes on the grid. The model of the tube furnace used was a Carbolite MTF 10/25/130. The exact dimensions of the CVD setup are given in figure 2.

2.3 Computational Modelling

The computation modelling was carried out to understand the flow field and the temperature distribution within the furnace tube where CNT growth had taken place. This has provided an insight into the CNT deposition process and in-depth understanding of growth conditions inside the heating chamber of the furnace.

2.3.1 Computational Geometry

The computational geometry includes the furnace tube, glass fittings at each end and connection tubes at the inlet and outlet. The extension of the computational geometry beyond the furnace tube avoided end effects due to sudden expansion and contraction at the gas at either end. The computational domain used for the simulations is shown in figure 3. To simplify the problem, we have not included the steel strip used for CNT deposition as in the CNT growth experiments. This allowed the computational geometry to be axisymmetric reducing computational time significantly but enabling to understand the growth in detail.

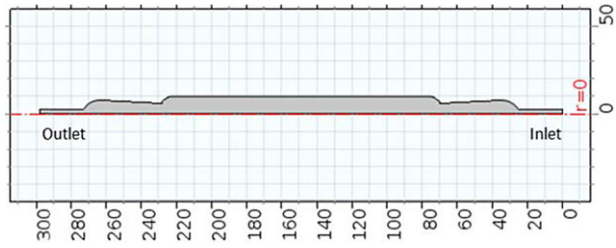

Fig. 3 The computational geometry of the furnace tube and connections. All dimensions are in mm and in correlation with figure 2.

2.3.2 Governing Equations

The optimum flow rate for CNT deposition was found to be 0.25 SLPM which corresponds to a Reynolds number of approximately 20. The governing equations are the continuity and incompressible Navier-Stokes equations for laminar flow fully coupled with heat equation for heat transfer. The temperature dependence of the fluid properties (i.e. density and viscosity) of the gas mixture provided by EffecTech Ltd. was incorporated in to the model using algebraic equations. The problem was solved in dimensional form at steady state. The fluid flow equations were specified as follows:

$$\nabla \cdot u = 0 \tag{1}$$

$$\rho(\boldsymbol{u} \cdot \nabla)\boldsymbol{u} = \nabla \cdot [-pI + \eta(\nabla \boldsymbol{u} + \nabla \boldsymbol{u}^T)] \tag{2}$$

where $\boldsymbol{u}$, p, I, ρ and η denotes the velocity field, pressure, identity matrix, density and dynamic viscosity respectively. The heat equation is given by

$$\rho C_p u.\nabla T = \nabla.(k\nabla T) \tag{3}$$

where T, C_p and k denotes temperature, heat capacity at constant pressure and thermal conductivity of the fluid respectively.

2.3.3 Boundary Conditions

The boundary conditions for the fluid flow were set as follows: (i) no slip boundary conditions on the glass walls; (ii) normal gas velocity corresponding to the volumetric flow rate at the inlet; (iii) pressure boundary condition at the outlet. For the heat transfer boundary conditions: (iv) inlet gas temperature was set to ambient temperature; (v) outlet boundary conditions were set as $-n.(-k\nabla T) = 0$ (vi) The internal surface temperature of the furnace tube was set according to White and King (2009), considering the cooling effects at the entrance due to gas flow. An additional simulation was carried out with a symmetric temperature profile provided by the manufacturer (for a stationary fluid inside the tube).

2.3.4 Numerical Method

The problem was solved using a commercial finite element code - Comsol Multiphysics^{TM} 5.0. Mesh-independent solutions were obtained with 196484 triangular elements and confirmed using a higher mesh density of 650972 elements. The number of degrees of freedom (DOFs) solved for was 423220. The total simulation time was approximately 38 s on an Intel Core i7 64-bit 2.7 GHz processor.

3 Results and discussion

An image of the sample prepared by CVD of the blast furnace is shown in figure 4. Notably, the CNT growth has only taken place on the steel substrate, and no deposition was observed on the quartz tube. This suggested that the steel itself may be acting as the catalyst for CNT growth when the blast furnace gas is used as the carbon source. A recent study has shown that steel can act as the catalyst for CNT growth, as it contains elements such as Fe, Co, Ni etc, which are all known to catalyse

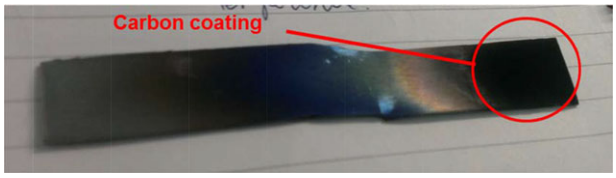

Fig. 4 Image of steel after chemical vapour deposition of blast furnace gas at a furnace temperature of 825 °C and gas flow rate of 250 ml/min for 30 mins.

CNT growth. [22] The ability to grow CNTs on the steel surface eliminates the need of purposely designed expensive catalysts and simplifies the CNT growth significantly compared to the methods reported previously. [10, 22] In terms of low-cost CNT production at manufacturing scale, this is a key finding as steel is widely available at low-cost and is robust and stable. As illustrated by the image of the steel substrate in figure 4, only the substrate end which was closest to the gas inlet nozzle was coated with carbon. The area of black carbon coating was approximately 20×15 mm (i.e. along a 20 mm section from the leading edge). It was initially thought that the deposition of carbon took place only at the front end of steel strip due to the temperature gradient at the entrance to the tube furnace (which can drop by ~25 °C at either end of the furnace compared to that of at the center, according to the operational temperature profile provided by the furnace manufacturer Carbolite Ltd). [24] However, further experiments conducted by repeating the process at lower and higher temperatures by steps of 25 °C from the set temperature of 825 °C did not show any notable changes in the position of the carbon layer. A recent study has shown that the cooling effect from precursor gas flow (which is essentially at room temperature before it enters the heated chamber) can result in a steep temperature gradient from the center to the leading edge of the tube furnace which can be in the order of a few hundred degrees within few centimeters distance. [25] Therefore, it is possible that the CNTs have only grown at the front end of the steel substrate where the density is just high enough to provide a sufficient collision frequency of CO_2 molecules with the steel substrate. As the flue gas flows towards the middle section of the furnace, the gas can expand significantly under the increasing temperature thereby reducing the contact probability of carbon source gas molecules with the steel substrate. To validate this hypothesis, CFD simulations were conducted in order to determine the flow and temperature profiles within the tube furnace. These profiles, with and without taking into account the cooling effect of the gas flow, are shown in the figures 5 and 6, respectively.

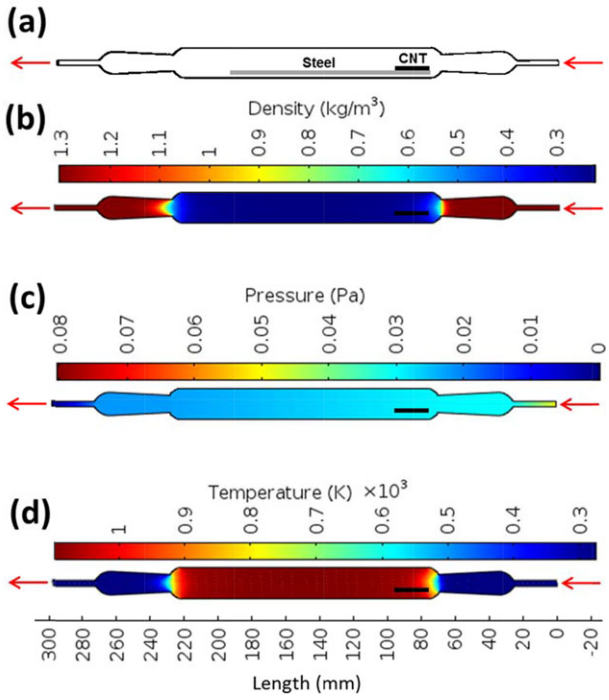

Fig. 5 (a) schematic diagram of the quartz tube used for the CNT growth from the blast furnace gas, indicating the size and position of the steel and CNT coating. (b), (c) and (d) show the simulated density, pressure and temperature profiles, respectively, inside the tube when the furnace was set to 825 °C, taking into account the temperature uniformity profile of the tube furnace. These are the profiles without taking into account the cooling effect of the gas flow. The red arrows indicate the direct of the gas flow (250 ml/min), and the black bars represent the area in which the CNT growth takes place.

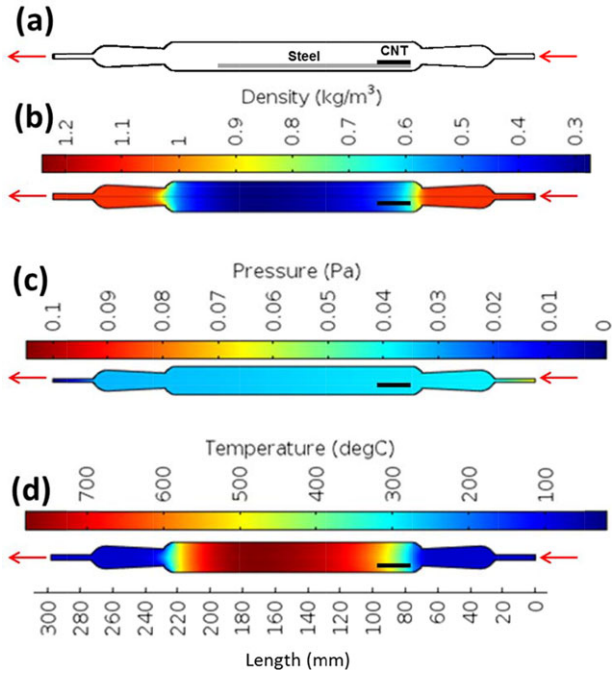

Fig. 6 (a) schematic diagram of the quartz tube used for the CNT growth from the blast furnace gas, indicating the size and position of the steel and CNT coating. (b), (c) and (d) show the simulated density, pressure and temperature profiles, respectively, inside the tube when the furnace was set to 825 °C, taking into account the temperature uniformity profile of the tube furnace, as well as the cooling effect of the gas flow. The red arrows indicate the direct of the gas flow (250 ml/min), and the black bars represent the area in which the CNT growth takes place.

The simulations show that in the region where the CNT growth took place (along the first 20 mm of strip at the front end of the tube), the temperature and hence the density of the gas varies significantly, suggesting that it could be the main reason for the CNT coating to occur only at the front end. As the CVD was carried out at atmospheric pressure, we believe that coating on the entire steel substrate may be achieved at an elevated pressure, in which the density of the carbon source can be maintained at sufficiently high levels to achieve CNT growth; however, such a study is beyond the scope of present work.

The morphological properties of carbon coating were studied by SEM and TEM which are shown in figures 7 and 8, respectively. It can be seen that CNTs adopt a highly random and entangled morphology on the steel substrate. The CNTs have a relatively low density with large voids. Based on the TEM images, it is evident that the CNTs are multi-walled, with the number of walls ranging from 7 to 14. The carbon coated steel was characterized by Raman spectroscopy, the spectrum is shown in figure 9. Typically there are four main features in the Raman spectra of a carbon nanotube samples – the radial breathing mode (RBM) region, the D-band, the G-band and the G'-band. The D band arises due to defects, the G band is due to the in-plane vibration of graphite and the G' band is a second order harmonic of the G band. Typically, RBMs are only observed for single-walled carbon nanotubes (SWCNTs) as RBMs cannot be detected for tube diameters >2 nm, therefore the signal for the outer wall in MWCNTs is too weak to be detected and the signal for the inner tubes is too broad. [26] The ratio of the D/G band intensities gives an indication of the quality of the carbon nanotubes. From observation of the Raman spectrum it is apparent that the CNTs are high in defects with the ratio of D/G in the range of 1.90. Also, surprisingly, the presences of three RBM peaks are observed at 215, 275 and 383 cm^{-1}. Some previous reports

CRYSTAL Research & Technology

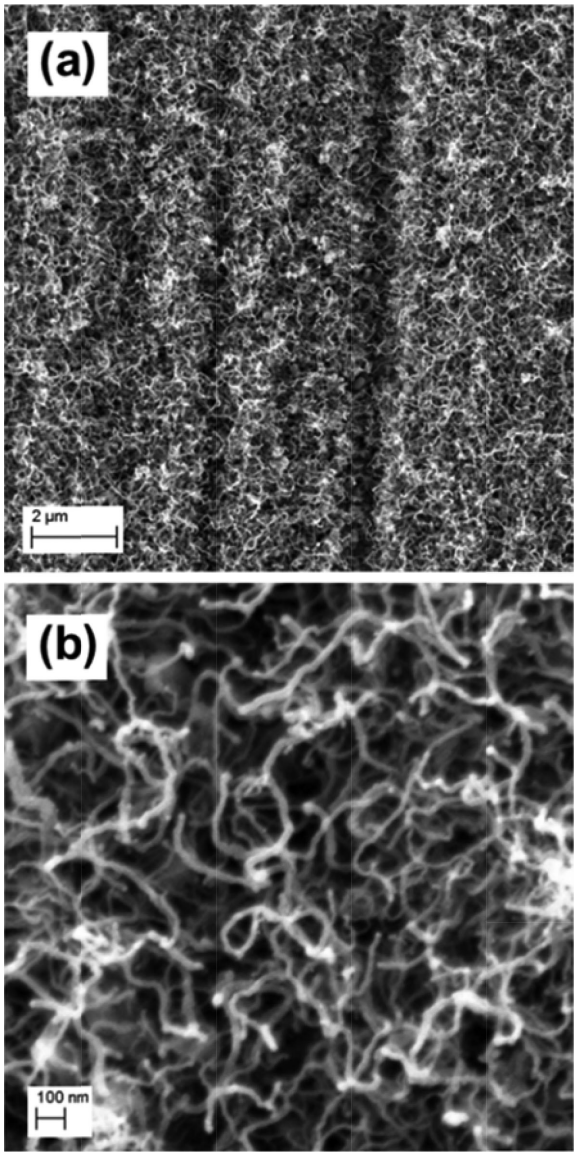

Fig. 7 SEM images of CNTs grown steel substrate by CVD of blast furnace gas.

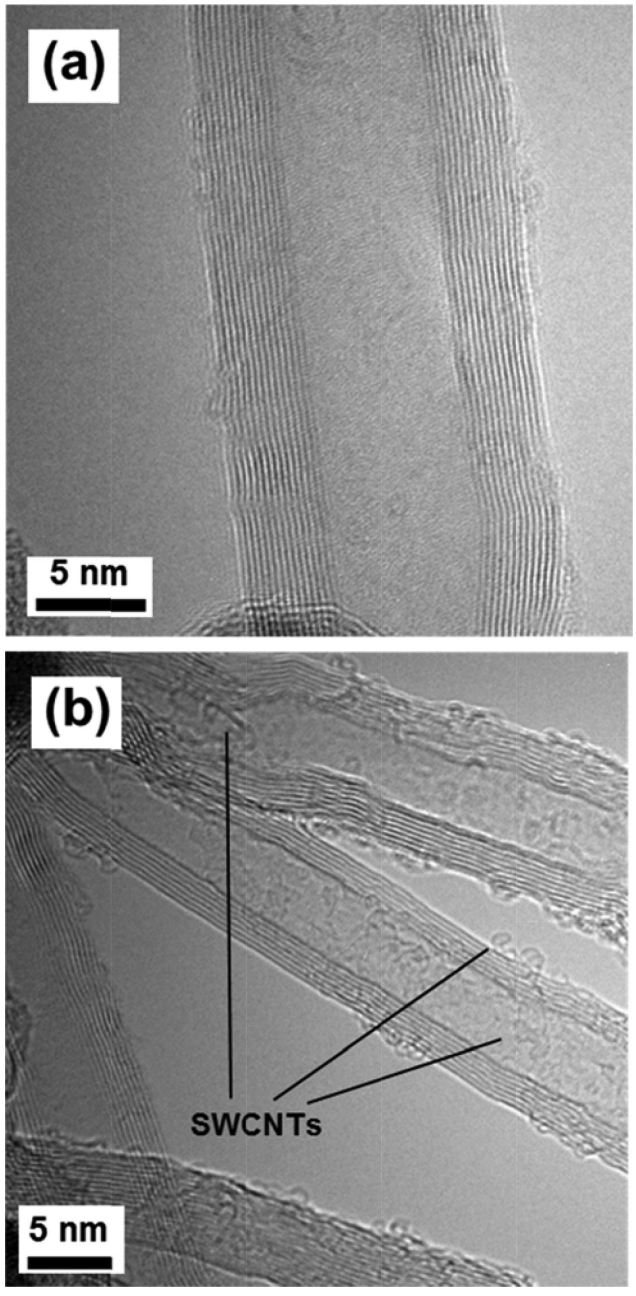

Fig. 8 TEM images of CNTs grown steel substrate by CVD of blast furnace gas.

have argued that the presence of RBMs in MWCNTs can be due to the vibration of the atoms of the inner shell of the MWCNT; [27, 28] however, this is unlikely in our case as the diameters of the inner walls of the CNTs by this method are in the order of 5 nm or larger. Gupta et al. have shown that the presence of SWCNTs inside the cavity of MWCNTs can give RBM peaks, which was the first report of such evidence. [29] Further analysis of figure 8b identified that there are in fact SWCNTs inside the cavity of the MWCNT, therefore this is the most likely reason for the presence of RBMs in the Raman spectrum of our samples.

The middle region of the steel strip which appeared to be uncoated with carbon had turned to a purple color (figure 4). This area was also analyzed by Raman spectroscopy to determine if the nature of the steel surface had been changed during the CVD process. The Raman spectrum is shown in figure 10. It was found that Raman spectrum of this purple region matched the Raman spectrum of magnetite, Fe_3O_4, giving peaks at 304, 520 and 660 cm^{-1}.

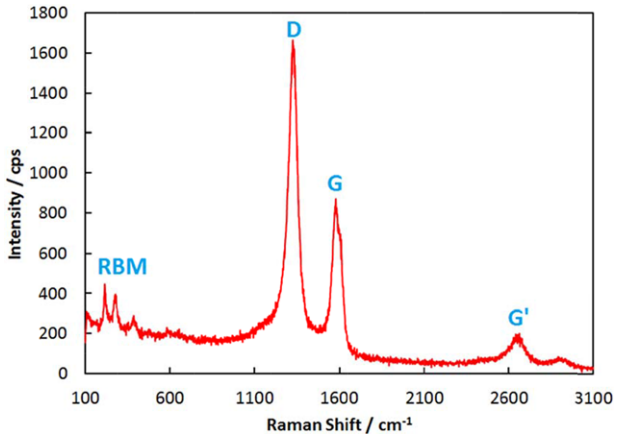

Fig. 9 Raman spectrum of CNTs on the steel substrate after 30 mins of CVD of blast furnace gas.

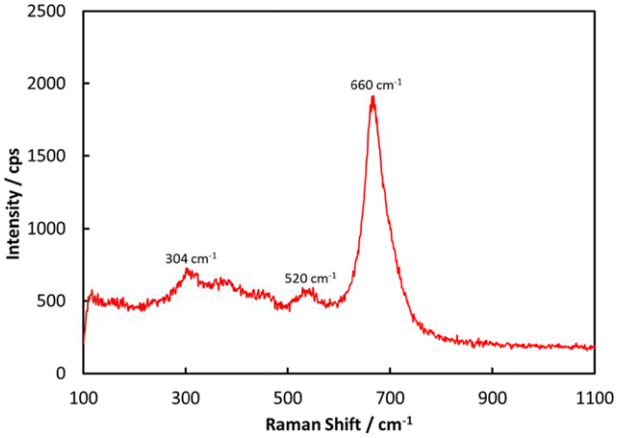

Fig. 10 Raman spectrum of the purple region of the steel strip after CVD of blast furnace gas mixtures at 825 °C at a flow rate of 250 ml/min for 30 mins.

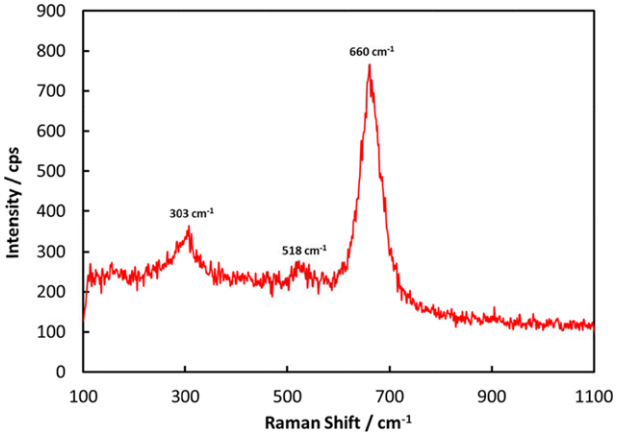

Fig. 11 Raman spectrum for shiney grey coating on steel after CVD of pure CO_2 at 825 °C at a flow rate of 250 ml/min for 30 mins.

Also, a control experiment was conducted using pure CO_2 under the same experimental conditions in order to establish whether CNT growth takes place when pure CO_2 is used as the carbon source. There was no CNT growth indicating that the CO and H_2 are necessary in facilitating the reducing atmosphere necessary for the growth; [30] typical blast furnace gases contain these component gases. Interestingly, when pure CO_2 was used, the surface of the steel turned to a shiny grey color. The surface of steel strips used for controlled experiment was investigated by Raman spectroscopy and it matched well with the spectrum for magnetite as shown in figure 11.

4 Conclusions

Our studies demonstrate that waste and environmental pollutant blast furnace gases from the iron and steel industry, which consist mainly of CO_2, CO, N_2 and H_2, can directly be used to grow CNTs on steel substrates at 825 °C and atmospheric pressure with no modification to the gas composition. The CNT growth only took place on one end of the steel substrate. Computational modelling confirmed that the reason for this was due to a rapid decrease in the gas density as it travels further into the heated tube. The steel itself acts as the catalyst (in addition to facilitating as the substrate) for CNT growth. This eliminates the need of purposely designed catalysts and simplifies the CNT growth significantly compared to the methods reported previously. The CNTs can be removed from the steel substrate, purified and then be directly used in an appropriate application. The steel substrates can also be reused. The method is potentially scalable for low-cost CNT production targeting a range of applications in which CNTs are currently in high demand. Alternatively, the CNT coated steel substrates can also be directly used as electrodes for electrochemical energy storage devices such as batteries or supercapacitors or as bipolar plates for fuel cells. [8, 9, 23, 31–33]. In general, our findings show that waste blast furnace gas, which is a key contributor to environmental pollution, can be successfully utilized for the production of commercially valuable materials and bring wider benefits (i.e. economic, environmental, social, political) to the society.

Acknowledgements. JS would like to thank Tata Steel for the partly funded PhD Studentship which enabled this work to be carried out. Loughborough University is also acknowledged for the remaining funding for the PhD studentship. KGUW acknowledges the support received from the Engineering and Physical Sciences Research

Council (Grant no. EP/H020543/1). The authors acknowledge use of the facilities and the assistance of Dr. Zhaoxia Zhou for TEM measurements in the Loughborough Materials Characterisation Centre. All authors would like to thank EffecTech Ltd for supplying the gas mixtures and conducting gas chromatography measurements.

Key words. Blast furnace, Carbon dioxide, Carbon nanotube, Carbon monoxide, CVD, Steel.

References

[1] K. Han, C.K. Ahn, M.S. Lee, Performance of an ammonia-based CO2 capture pilot facility in iron and steel industry, Int. J. Greenh. Gas Control. **27** (2014) 239–246.

[2] M. Kundak, L. Lasic, J. Crnko, CO2 Emissions in the Steel Industry, Metalurgija. **48** (2009) 193–197.

[3] D.Y.C. Leung, G. Caramanna, M.M. Maroto-Valer, An overview of current status of carbon dioxide capture and storage technologies, Renew. Sustain. Energy Rev. **39** (2014) 426–443.

[4] S. Chopra, K. McGuire, N. Gothard, A.M. Rao, A. Pham, Selective gas detection using a carbon nanotube sensor, Appl. Phys. Lett. **83** (2003) 2280.

[5] S. Rul, F. Lefèvre-schlick, E. Capria, C. Laurent, A. Peigney, Percolation of single-walled carbon nanotubes in ceramic matrix nanocomposites, Acta Mater. **52** (2004) 1061–1067.

[6] M. Yu, H.H. Funke, J.L. Falconer, R.D. Noble, High density, vertically-aligned carbon nanotube membranes., Nano Lett. **9** (2009) 225–9.

[7] V. Lordi, N. Yao, J. Wei, Method for Supporting Platinum on Single-Walled Carbon Nanotubes for a Selective Hydrogenation Catalyst, Chem. Mater. **13** (2001) 733–737.

[8] C. Du, N. Pan, Supercapacitors using carbon nanotubes films by electrophoretic deposition, J. Power Sources. **160** (2006) 1487–1494.

[9] C. Masarapu, V. Subramanian, H. Zhu, B. Wei, Long-Cycle Electrochemical Behavior of Multiwall Carbon Nanotubes Synthesized on Stainless Steel in Li Ion Batteries, Adv. Funct. Mater. **19** (2009) 1008–1014.

[10] J.S. Sagu, K.G. Upul Wijayantha, M. Bohm, S. Bohm, T.K. Rout, Aerosol-Assisted Chemical Vapor Deposition of Multi-Walled Carbon Nanotubes on Steel Substrates for Application in Supercapacitors , Adv. Eng. Mater. (2015) n/a–n/a.

[11] J.A. Isaacs, A. Tanwani, M.L. Healy, L.J. Dahlben, Economic assessment of single-walled carbon nanotube processes, J. Nanoparticle Res. **12** (2009) 551–562.

[12] Global Carbon Nanotubes Market 2014-2018: ReportsnReports, 2013. http://www.reportsnreports.com/reports/270702-global-carbon-nanotubes-market-2014-2018.html (accessed October 6, 2014).

[13] H. Dai, A.G. Rinzler, P. Nikolaev, A. Thess, D.T. Colbert, R.E. Smalley, Single-wall nanotubes produced by metal-catalyzed disproportionation of carbon monoxide, Chem. Phys. Lett. **260** (1996) 471–475.

[14] P. Chen, H.-B. Zhang, G.-D. Lin, Q. Hong, K.R. Tsai, Growth of carbon nanotubes by catalytic decomposition of CH4 or CO on a Ni−MgO catalyst, Carbon N. Y. **35** (1997) 1495–1501.

[15] Y. Tang, Y. Zheng, C. Lee, N. Wang, S. Lee, T. Sham, Carbon monoxide-assisted growth of carbon nanotubes, Chem. Phys. Lett. **342** (2001) 259–264.

[16] B. Zheng, C. Lu, G. Gu, A. Makarovski, G. Finkelstein, J. Liu, Efficient CVD Growth of Single-Walled Carbon Nanotubes on Surfaces Using Carbon Monoxide Precursor, Nano Lett. **2** (2002) 895–898.

[17] T. Reda, C.M. Plugge, N.J. Abram, J. Hirst, Reversible interconversion of carbon dioxide and formate by an electroactive enzyme., Proc. Natl. Acad. Sci. U. S. A. **105** (2008) 10654–8.

[18] M. Motiei, Y.R. Hacohen, J. Calderon-Moreno, A. Gedanken, Preparing Carbon Nanotubes and Nested Fullerenes from Supercritical CO2 by a Chemical Reaction, J. Am. Chem. Soc. **123** (2001) 8624–8625. http://pubs.acs.org/doi/pdf/10.1021/ja015859a (accessed September 17, 2014).

[19] Z. Lou, Q. Chen, W. Wang, Y. Zhang, Synthesis of carbon nanotubes by reduction of carbon dioxide with metallic lithium, Carbon N. Y. **41** (2003) 3063–3067.

[20] M.H. Khedr, M. Bahgat, M.I. Nasr, E.K. Sedeek, CO2 decomposition over freshly reduced nanocrystalline Fe2O3, Colloids Surfaces A Physicochem. Eng. Asp. **302** (2007) 517–524.

[21] M.H. Khedr, A.A. Farghali, Microstructure, kinetics and mechanisms of CO2 catalytic decomposition over freshly reduced nano-crystallite CuFe2O4 at 400–600 °C, Appl. Catal. B Environ. **61** (2005) 219–226.

[22] A. V. Gaikwad, T.K. Rout, D. Van der Plas, R. V. Dennis, S. Banerjee, S. Pacheco Benito. et al., Carbon nanotube/carbon nanofiber growth from industrial by-product gases on low- and high-alloy steels, Carbon N. Y. **50** (2012) 4722–4731.

[23] Y. Show, K. Takahashi, Stainless steel bipolar plate coated with carbon nanotube (CNT)/polytetrafluoroethylene (PTFE) composite film for proton exchange membrane fuel cell (PEMFC), J. Power Sources. **190** (2009) 322–325.

[24] Carbolite, Carbolite Laboratory Furnaces Data Sheets, (n.d.). https://acs.expoplanner.com/files/acsfall10/ExhibFiles/1038_828_CarboliteTubeFurnaces.pdf (accessed June 10, 2015).

[25] R. White, D. King, Combined Experimental and Simulation (CFD) Analysis on Performance of a Horizontal Tube Reactor used to Porduce Carbon Nanotubes, Seventh Int. Conf. CFD Miner. Process Ind. (2009) 1–5.

[26] M.S. Dresselhaus, G. Dresselhaus, R. Saito, A. Jorio, Raman spectroscopy of carbon nanotubes, Phys. Rep. **409** (2005) 47–99.

[27] X. Zhao, Y. Ando, L.-C. Qin, H. Kataura, Y. Maniwa, R. Saito, Radial breathing modes of multiwalled carbon nanotubes, Chem. Phys. Lett. **361** (2002) 169–174.
[28] H. Jantoljak, J.-P. Salvetat, L. Forró, C. Thomsen, Low-energy Raman-active phonons of multiwalled carbon nanotubes, Appl. Phys. A Mater. Sci. Process. **67** (1998) 113–116.
[29] R. Gupta, B.P. Singh, V.N. Singh, T.K. Gupta, R.B. Mathur, Origin of radial breathing mode in multiwall carbon nanotubes synthesized by catalytic chemical vapor deposition, Carbon N. Y. **66** (2014) 724–726.
[30] M. Hashempour, A. Vicenzo, F. Zhao, M. Bestetti, Direct growth of MWCNTs on 316 stainless steel by chemical vapor deposition: Effect of surface nano-features on CNT growth and structure, Carbon N. Y. **63** (2013) 330–347.
[31] L. Kou, T. Huang, B. Zheng, Y. Han, X. Zhao, K. Gopalsamy. et al., Coaxial wet-spun yarn supercapacitors for high-energy density and safe wearable electronics., Nat. Commun. **5** (2014) 3754.
[32] D. Yu, K. Goh, H. Wang, L. Wei, W. Jiang, Q. Zhang. et al., Scalable synthesis of hierarchically structured carbon nanotube-graphene fibres for capacitive energy storage., Nat. Nanotechnol. **9** (2014) 555–62.
[33] S.W. Lee, N. Yabuuchi, B.M. Gallant, S. Chen, B.-S. Kim, P.T. Hammond. et al., High-power lithium batteries from functionalized carbon-nanotube electrodes., Nat. Nanotechnol. **5** (2010) 531–7.

